Optics & Laser Technology 48 (2013) 495–502

Contents lists available at SciVerse ScienceDirect

Optics & Laser Technology

journal homepage: www.elsevier.com/locate/optlastec

Numerical and experimental comparison of an all-fiber APM laser with two-coupled linear cavities

E. Paulucci [a,b,*], N.A. Russo [a], E.E. Sicre [c], R. Duchowicz [a,b]

[a] Centro de Investigaciones Opticas (CONICET-CIC), Cno. Centenario 505 y 508, Gonnet (C.P. 1897), Buenos Aires, Argentina
[b] Depto. de Electrotecnia. Fac. de Ingeniería, Universidad Nacional de La Plata, Calle 48 y 115. La Plata (C.P. 1900), Buenos Aires, Argentina
[c] Intec, Universidad Argentina de la Empresa, Lima 717, Ciudad Autónoma de Buenos Aires C1073AAO, Buenos Aires, Argentina

ARTICLE INFO

Article history:
Received 10 July 2012
Received in revised form
21 November 2012
Accepted 25 November 2012

Keywords:
Fiber lasers
Modulation tunning and mode locking
Gratings

ABSTRACT

In this work, some properties of a two coupled cavities all-fiber laser as a function of the ratio between their optical lengths are analyzed. The laser is composed of an active primary cavity generated by an erbium-doped fiber and two fiber Bragg gratings (FBG_1 and FBG_2), and a passive cavity made with an appropriate length of standard optical fiber spliced to FBG_2 and employing the Fresnel reflection at the other end of the pigtail. The operation of this additive-pulse mode-locking (APM) laser is based on the coherent addition of pulses that interact on a central reflective element which is a common component for both cavities. The developed model considers the propagation of electric fields into the system solving the non-linear Schrödinger equation (NLSE) through the Split-Step Method (SSM). Reflectivity and transmittance characteristics of the FBGs used as feedback elements are simulated by using the Transfer-Matrix Method (TMM). The main system parameters employed on the calculations are: group velocity dispersion (GVD), self-phase modulation (SPM), gain factor that includes the effects of self-saturation, fiber losses and dispersion of the FBGs. Numerical results for the pulse width and the peak power of the output, obtained from the application of the numerical model, are compared with experimental values measured by varying the length of the auxiliary cavity. A good agreement between them is observed. When the auxiliary cavity length is reduced with respect to the main cavity length, both experimental and numerical results show a decrease in the temporal width with a corresponding increase in the repetition frequency of the pulses. If the main cavity length is made two or three times larger than the original one by varying the pigtail length, some of the laser output frequencies previously obtained are also founded. In that cases, similar values of the pulse width were found. This pulse width dependence with the repetition frequency was also verified by applying our mathematical model.

1. Introduction

Additive pulse mode-locking or coupled cavity mode-locking, is an all-optical, interferometric method which may produce short pulses at high repetition rates. Most works on APM are related with ultra-short pulse and optical combs generation for different applications in communications, and for introducing new experimental techniques in the field of optical metrology [1–4]. Passive APM lasers were first developed as bulk systems, but later they were improved as all-fiber configurations by employing different schemes based on doped fibers and filters such as FBGs [5–7]. These systems allow reaching moderate pulse intensities. Pulse widths of APM lasers can be in the range of picoseconds or less, with the help of a wide variety of compressing techniques [8–11]. In general, by employing active modulation techniques, it is possible to obtain high pulse intensities with low jitter levels. Today, APM hybrid lasers take advantages of active and passive systems, implemented with Er, Yb and double-cladding fibers together with optical modulators and/or filters, that allow reaching high powers with pulse durations in the range of femtoseconds [12–14].

The analytic methods employed to solve the output of this kind of APM lasers vary depending on the required degree of approximation of the results. Generally, the electric field envelope is calculated by a master equation that depends on simple parameters such as: gain/loss factors, dispersion and non-linearity of the fibers involved into the system and the reflectivity or transmission coefficients of filters/mirrors [15,16]. However, in some cases this model cannot be successfully used, in particular when the light signals have a large bandwidth, for example, in

* Corresponding author at: Depto. de Electrotecnia. Fac. de Ingeniería, Universidad Nacional de La Plata, Calle 48 y 115. La Plata (C.P. 1900), Buenos Aires, Argentina. Tel.: +54 221 4842759x207.
E-mail address: emanuelp@ciop.unlp.edu.ar (E. Paulucci).
URL: http://www.ciop.unlp.edu.ar (E. Paulucci).

0030-3992/$ - see front matter © 2012 Elsevier Ltd. All rights reserved.
http://dx.doi.org/10.1016/j.optlastec.2012.11.029

ultra-short pulse lasers and/or in the generation of optical combs by four-wave mixing (FWM) [17–19]. Modeling of these systems, involving linear and non-linear processes inside the laser cavity which should be precisely described, becomes a complex problem. Among others, we mention a precise description of the several dispersion profiles and the wavelength dependence of both, the group velocity and the non-linear terms.

Numerical models used to calculate the electric field propagation through the laser systems are focused to solve the NLSE [20]. Generally, a Runge–Kutta method is employed to find a solution in a system which is described by using simple parameters [15,21]. However, in other systems the boundary conditions require a full representation of the feedback elements, increasing the model complexity and the computational cost. As a solution of this problem, the SSM with variable steps works good, reaching accurate solutions in less time, and giving some advantages that enable an easy coupling of the electric fields by means of the TMM, as it will be described later.

In this work we present a numerical model that solves the output of an APM fiber laser consisting of two linear coupled cavities. The model give some solutions related to pulsed regimes, but other operating modes as the CW mode could be easily analyzed. The calculation of the electric fields propagation in both cavities is done by using the SSM [20,22], while their coupling is performed by employing the TMM [23,24]. The solution of the model is found by successive approximations, until a stable solution is reached when the intensity and shape of the pulses remain unchanged [6]. In our model, the transmission and reflection coefficients of the FBG used as some of the mirrors in the cavities were expressed in modulus and phase. This methodology is important for most APM systems because the solutions depend on variations of linear and non-linear phase, both related to GVD and SPM processes, optical path differences and group delays of the FBGs. Under our experimental conditions, a relationship was found between the pulse repetition frequency and its temporal width. This frequency (for a fixed main cavity length) is defined by the auxiliary cavity length. Results obtained by applying our model were compared with the experimental results and a good correlation between them was found.

The work is outlined as follows: In Section 2, we briefly sketch the APM technique and describe the laser model used in the work. Numerical procedure and computer simulations that illustrate the laser output employing different relationships between the cavity lengths are presented in Section 3. Experimental results are shown in Section 4, where a comprehensive analysis related with the effect of the main cavity length on the repetition frequency and temporal pulse width is included. In Section 5, a discussion about the comparison between simulated and experimental results is performed. Finally, our conclusions are presented in Section 6.

2. Theoretical model

The APM laser setup includes two linear coupled cavities, as shown in Fig. 1. The main cavity (active) is formed by certain length of erbium-doped fiber, limited by two uniform FBGs. The auxiliary cavity is made with a piece of standard SMF spliced to one of the gratings, and the other end is cut perpendicularly to the fiber axis to produce a Fresnel reflection of 4%. Usually, the APM technique is based on a non-linear external cavity that is coupled to the main laser cavity in a common mirror where a coherent interference process generates pulse narrowing. In our case, due to the low reflectivity value obtained from the pigtail end, the non-linear effect is mostly produced by the main cavity. This cavity produces equally-frequency-spaced modes at

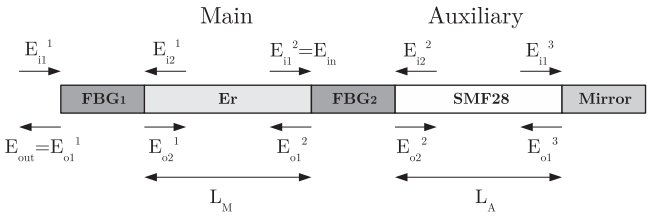

Fig. 1. Additive pulse mode-locking laser scheme. E_{in} and E_{out} are the electric field amplitudes of the input and output, respectively.

$\Delta f_M = c/(2n_0L_M)$, while the modes generated by the auxiliary cavity are spaced in $\Delta f_A = c/(2n_0L_A)$ (where L_M and L_A are the main and auxiliary cavity length values, respectively). In order to generate and analyze stable pulsed outputs, we changed the auxiliary cavity length L_A, which must satisfy the following condition:

$$\frac{L_M}{L_A} = \frac{N}{M} = k \tag{1}$$

where N and M are positive integers ($N \geq M$), as was described in our previous work [25]. When k is a fractional number, ratio of two co-prime numbers, the coupled cavities produce a stable beat between both frequencies. This process establishes the repetition rate of the pulsed emission. On the other way, conditions for mode-locking are particularly given by the gain medium (coherent emission) and Kerr effect in the excited doped fiber. Earlier attempts to mode-lock a laser in a three-mirror setup, where a minimal mismatch between both cavities was required, presented high difficulties. As Huang et al. [6] showed in their work, by using Bragg gratings as cavity mirrors, larger cavity mismatch can be tolerated.

Propagation of an electric field into an optical fiber can be analyzed by the NLSE [20]. As in [6,7], we define an operator whose coefficients are integrated over the propagation length $z=L$. Assuming that the error of this approximation is negligible for small increments δL, we can rewrite the NLSE as follows:

$$\hat{O}(\cdot) = i\frac{\alpha L}{2}(\cdot) + \frac{\beta_2 L}{2}\frac{\partial^2(\cdot)}{\partial t^2} - \gamma L|(\cdot)|^2(\cdot) \tag{2}$$

where $\alpha = \alpha_0$ is the fiber attenuation coefficient for the auxiliary cavity and $\alpha = g$ represents the gain in the active cavity, β_2 is the chromatic dispersion coefficient and γ is the non-linear parameter of the fiber, while this operator is applied to an electric field $E(z=0,t)$ through $(\cdot)$ to obtain an output field $E(z=\delta L,t)$. The independent variables of time t and propagation length z are neglected to simplify the notation in the following analysis.

In our model, this operator is solved through the SSM with variable step, in order to calculate the dispersion of pulses in the frequency domain and the non-linear phase in the time domain. To calculate the propagation in both cavities we have considered that the SSM supports small phase errors on the order of 0.1×10^{-3} rad and tolerances $||E_s - E_{s-1}||/||E_{s-1}|| < 1\%$ for $s = 1,\ldots,S$ calculated steps [26]. Due to the high reflectivity values ($>90\%$) used in the setup, the round trip time is much smaller than the average life time of a photon inside the active cavity. Our model allows describing the interaction of linear processes (GVD and dispersion of FBGs) and non-linear (SPM) related with soliton propagation inside the laser and it is able to determine the electric field solutions in other parts of the system.

Reflection and transmission characteristics of the FBGs (in amplitude and phase), and particularly the coupling of both electric fields on the central FBG, are calculated by using TMM. Then, the output electric field is obtained by applying the transmission coefficient of the FBG $_1$. The FBGs properties are defined by a square matrix U, where E_{ik} and E_{ok} are the input/output electric fields which are uniquely characterized by the

matrix elements U_{mn} with $m=$ 1,2. and $n=$ 1,2., where $k=$ 1,2. represents each port of the device, so that

$$\begin{bmatrix} E_{o1} \\ E_{o2} \end{bmatrix} = \begin{bmatrix} U_{11} & U_{12} \\ U_{21} & U_{22} \end{bmatrix} \begin{bmatrix} E_{i1} \\ E_{i2} \end{bmatrix} \tag{3}$$

The elements U_{mn} depend on the constructive parameters of the FBGs, such as the recorded period, the maximum variation of the refractive index and the physical length of the device [23]. Initially, we can express that the main diagonal elements are related to the reflection coefficients ρ, and the secondary diagonal elements are similar to the transmission coefficients τ of a FBG. It should be noted that to find the U_{mn} elements are necessary to assume that one of the fields of this equation vanishes. This is important to correctly define the characteristics of the fiber gratings. However, when the TMM is used to couple the electric fields into the laser, for example in our model at FBG_2, this condition (i.e. $E_{i2}=0$) cannot be applied because the field from the auxiliary cavity, although it has low intensity, produces a change in the phase profile of the coupled electrical fields. The coherent addition of these fields (or pulses) depends on their intensity and phase, even when the phase values are small (on the order of the working wavelength λ_0 or less). In this way, we can generalize the model with a system of non-linear equations such as

$$e^{-i\phi_m}\hat{O_m}U_{22_1}\hat{O_m}E_{o1} = E_{i1} \tag{4}$$

$$e^{i\phi_a}\hat{O_a}U_{11_3}\hat{O_a}E_{o2} = E_{i2} \tag{5}$$

where the subscript $d=1,2,3$ (device number) inside the U_{mn_d} operators represents the FGB's ($d=1,2.$) and the mirror ($d=3.$), while $\hat{O_m}$ and $\hat{O_a}$ are the propagation operators of the main and auxiliary cavities, respectively. Then, by replacing the output fields by Eq. (3) and rewriting the coupled equations of the system we can obtain

$$e^{-i\phi_m}\hat{O_m}U_{22_1}\hat{O_m}U_{11_2}E_{i1} - E_{i1} + e^{-i\phi_m}\hat{O_m}U_{22_1}\hat{O_m}U_{12_2}E_{i2} = 0 \tag{6}$$

$$e^{i\phi_a}\hat{O_a}U_{11_3}\hat{O_a}U_{21_2}E_{i1} + e^{i\phi_a}\hat{O_a}U_{11_3}\hat{O_a}U_{22_2}E_{i2} - E_{i2} = 0 \tag{7}$$

where the phases ϕ_m and ϕ_a are related with the optical lengths of the main and auxiliary cavities as follows:

$$\phi_{m,a} = 2\pi L_{m,a} n_0/\lambda_0 \tag{8}$$

Furthermore, the gain g of the system is quickly saturated, depending on the power of the generated pulses. In our model, the gain of the active medium g_0 is considered a constant, such that

$$g = g_0/(1+I_p/I_{sat}) \tag{9}$$

where g_0 represents the small signal gain of the active medium for the operation wavelength and depends on the applied pump power and the population levels of the doped fiber [16,27], $I_p = \int |E(t)|^2 dt$ is the integrated intensity of a pulse that it is present into the active medium and I_{sat} is the saturation intensity value (about 7 dBm in our model, that is a standard value as we can observe in [27]). Thus, when we are applying the SSM to solve the propagation in the active cavity, the gain value should be adequately adjusted, depending on the value of the pulse intensity inside this cavity.

With the previous representation, our model works as follows. At the beginning, an initial electric field $E_{in}=E_{i1}$ is used as input, which has a hyperbolic secant profile that is well known in mode-locking systems [28,29]. At this moment, the output is zero and the pulse is propagated within both cavities to complete a round-trip . Then these fields are quickly updated in an iterative mode to reach a stable solution, as we will see later. The elected criterion to determine a correct solution (in modulus and phase) is based on that the intensity and pulse width remains unchanged with the increment of the round-trip numbers, for an appropriate set of system parameters.

It should be noted that for each value of k, the algorithm implemented is slightly different. Specifically it is necessary to combine the electric fields from both cavities with an appropriate spatial and temporal synchronization. When the laser cavity lengths are the same ($k=1$), the input field E_{in} in Fig. 1 is transmitted to the auxiliary cavity and at the same time is reflected by counter-propagation into the main cavity. The resulting fields at the FBG_1 and the mirror are reflected toward the FBG_2, completing a round-trip . When the auxiliary cavity length is decreased, i.e. $k=2$, $E_{in}=E_{i1}^2$ is transmitted into the auxiliary cavity and is reflected by the mirror, being counter-propagated as E_{i2}^2. At the same instant, the field E_{o1}^2 has been propagated a distance L_M, by obtaining the field E_{i2}^1 at the FBG_1. The cycle is completed when the reflected field E_{o2}^1 is propagated on the main cavity until is updated the field E_{i1}^2, and E_{i2}^2 should be updated to be coupled to E_{i1}^2. In summary, the auxiliary cavity fields should be k times updated before coupling with the new field E_{i1}^2. This condition must be applied for any integer lengths ratio k, while for rational ratios (i.e. between co-primes numbers) the analysis becomes more complex.

3. Numerical results

The laser operation was analyzed by employing the theoretical model for a wavelength $\lambda_0=1553.55$ nm, effective refractive index equal to $n_0=1.46$ and the electric fields were sampled in time at $T_s=10$ ps and employing around 2^{18} points. In Table 1, we summarize the employed parameters.

The FBGs used in our model are assumed to be identical, and the reflectivity and dispersion characteristics can be seen in Fig. 2. It is important to note that, although the FBG dispersion values are small compared to those of a standard fiber, the output can change significantly due to them.

Related to the effect of the noise in our model, we applied a pulse with additive Gaussian noise at the input which is propagated through the system as we can see in Fig. 3. The noise was generated using the model of in phase and quadrature noise [30] and assuming a low signal-to-noise ratio at the input $SNR_{in}=0.1$ dB, by employing

Table 1
Model parameters.

Main cavity	Auxiliary cavity	FBGs and mirror
$L_M = 1.86\times10^6\lambda_0/n_0 = 1.976$ m	$L_M = L_A$	$\lvert\rho_1\rvert^2 = \lvert\rho_2\rvert^2 = 0.93$ and $\lvert\rho_3\rvert^2 = 0.04$
$g_0 = 0.2735$ m^{-1}	$\alpha_0 = 4\times10^{-5}$ m^{-1}	$\lambda_1 = \lambda_2 = 1553.55$ nm
$\beta_{2_M} = 108$ ps^2/km	$\beta_{2_A} = -20$ ps^2/km	$\Delta\lambda_{1,2_{3\ dB}} = 0.2$ nm
$\gamma_M = 4.5745\times10^{-3}$ W^{-1} m^{-1}	$\gamma_A = 1.6519\times10^{-3}$ W^{-1} m^{-1}	$\delta n_{1;2} = 11.5\times10^{-5}$
$A_{eff_M} = 78.54$ μm^2	$A_{eff_A} = 254.46$ μm^2	$L_{1;2} = 3.75\times10^3\lambda_0$

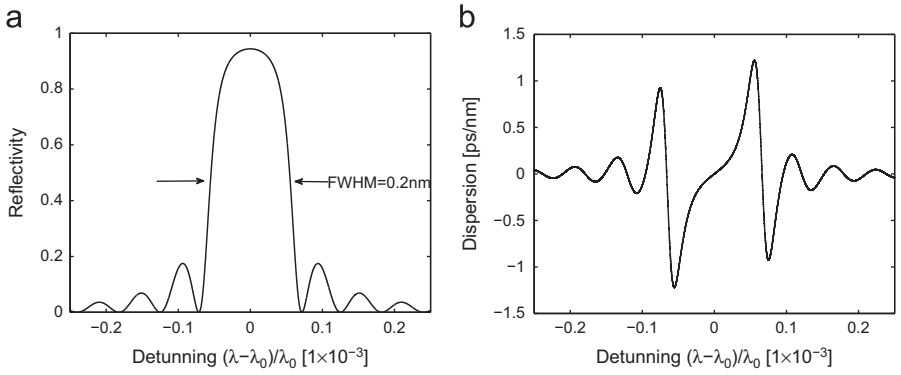

Fig. 2. FBG characteristics employed in our numerical model. (a) Reflectivity and (b) dispersion as a function of detuning.

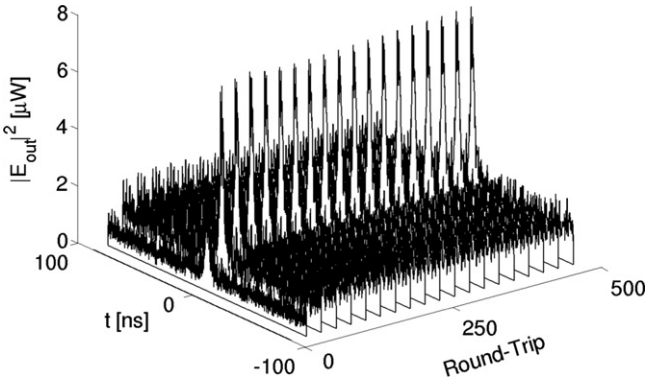

Fig. 3. Output electric field intensity evolution in the time domain (SNR=0.1 dB).

a pulse with a power of $P_{in} \approx -50$ dBm and a temporal width of about $T_{in} = 2$ ns. It can be seen that even under small SNR_{in} and for small levels of the gain g_0, the resulting pulse acquires an $SNR_{out} > SNR_{in}$, while the average temporal width was close to 3.5 ns with a moderate standard deviation related to the low value of SNR_{in}. For this case, the SNR_{out} was around 10 dB. It can also be noted the presence of the CW mode expressed by the background level of random noise introduced. Clearly, the noise does not change the global behavior of the solution. In the rest of the paper we do not consider any noise in order to reduce the calculation time. This election is based on the good values of SNR that were obtained in measurements made under the mode-locked condition.

In order to analyze the effect of changing the auxiliary cavity length (L_A), we applied the model to laser systems with k values equal to 1, 2, 3 and 4, keeping constant the length of the main cavity ($L_M = 1.976$ m). For most cases, a stable solution was found for a round-trip number larger than 100, where the phase of the electric field E_{i1}^2 took a stable value near to $-\pi/2$ [31]. However, we extended the simulations to 500 and 1000 round-trips to ensure the stability conditions. In all cases, we supposed that the pulse peak intensity inside the active medium (main cavity) was about $P_{in} \approx 20$ dBm, and the input pulse width used to start the calculations was around $T_{in} = 2$ ns.

The number of round-trip needed to find a stable solution can change depending on the parameters of Table 1 and the initial conditions of the input pulse. The characteristics of the latter, such as its intensity, temporal width and shape, are conveniently chosen to ensure a fast convergence. However, if the pulse entered has different attributes than those listed, the system takes care of auto-adjust these parameters reaching a result in an increased number of round-trips, at the expense of increasing the computation time. Besides, the value of g_0 in Table 1 was compatible with the experimental one and is in good agreement with the final power level of pulses.

Fig. 4 shows the numerical results for different values of k: (a) $k=1$, (b) $k=2$, (c) $k=3$ and (d) $k=4$, with $L_M = 1.976$ m for all cases. In Fig. 4(a) only appears one pulse because the propagation time for both cavities is identical. However, in the plots drawn in Fig. 4(b)–(d) appear 2, 3 or 4 pulses, respectively, in the same time window. As it was described before, this depends on the beat frequency between both cavities (or on the cavities lengths ratio), resulting on a particular solution for each case. The pulse widths obtained from the numerical results, were: (a) 3.46 ns, (b) 2.25 ns, (c) 1.74 ns and (d) 1.45 ns. On the other hand, we observed a broadening in the pulse bandwidth of around five times, justifying the existence of a moderate Kerr effect in our model. Fig. 5 shows how fast the pulse converge to its final stable form, for $k = 1$ and 2. In the first set of iterations, the pulse energy is increased with moderate steps, but then these increments get smaller until just before reaching a stable solution.

4. Experimental results

The experimental setup included a single mode 980/1550 nm wavelength division multiplexer (WDM) to couple the pump beam and to extract the generated fiber laser beam through the 1550 nm branch. This coupler was connected to the FBG_1 through the common 980/1550 nm branch. A pigtailed semiconductor laser (SDL Pump Module, model SDLO-2500-125) emitting at 975.12 nm, with 125 mW maximum output power and 0.5 nm of spectral bandwidth was used to pump the active medium. The main cavity was built with a piece of highly doped erbium fiber (LIEKKI Er30-4/125), which was completed with a bit of photosensitive optical fiber where the FBGs were written, to obtain the total length of $L_M = 1.976$ m. The doped fiber had 30 dB/m of peak absorption at 1530 nm, a mode field diameter of 6.5 μm at 1550 nm, a core numerical aperture of 0.2 and the cut-off wavelength in the range 800–980 nm. The auxiliary cavity was implemented with a piece of standard single mode fiber (SMF28) spliced to FBG_2. The free end of the pigtail was cut perpendicular to the fiber axis in order to obtain a 4% reflection coefficient. Both cavities lengths were measured with an error of ± 1 mm. When the lengths of the coupled cavities are not properly adjusted but they are within the mentioned tolerance, the system adjusts itself through the change produced in the effective penetration length of the FBGs [6].

The uniform fiber Bragg gratings (from O-ELAND) employed in this experimental setup were spliced at each end of the gain fiber and their spectral characteristics were measured with an Optical Spectrum Analyzer (Yokogawa AQ6370B). Both Bragg gratings

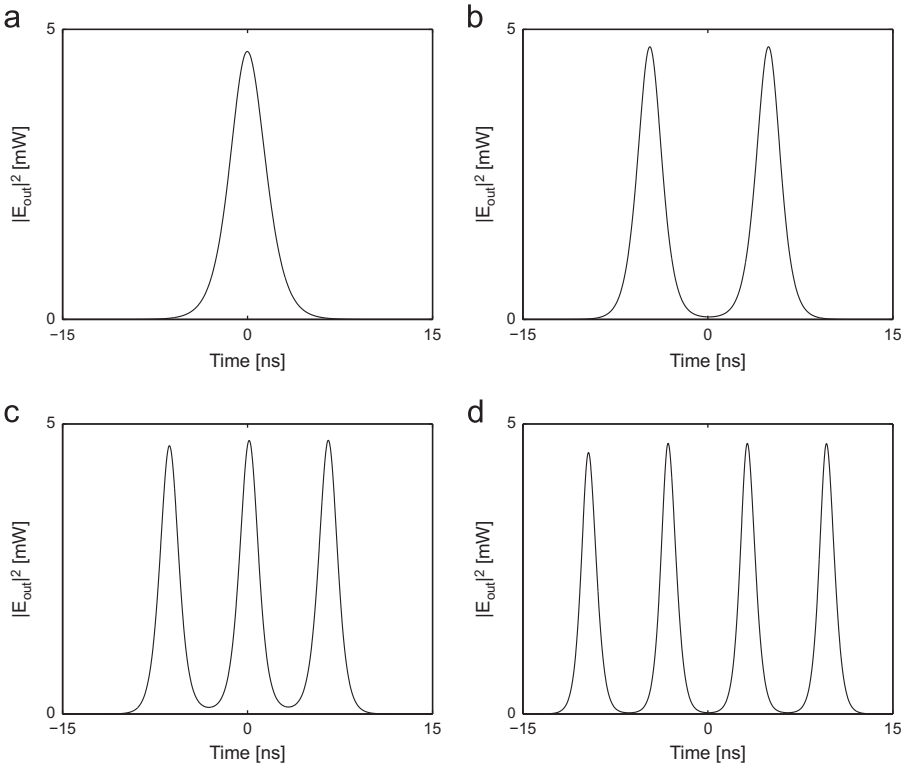

Fig. 4. Simulation of the squared modulus of the electric field for different length ratios k. (a) $k=1$ ($T_{out}=3.46$ ns), (b) $k=2$ ($T_{out}=2.26$ ns), (c) $k=3$ ($T_{out}=1.74$ ns) and (d) $k=4$ ($T_{out}=1.45$ ns).

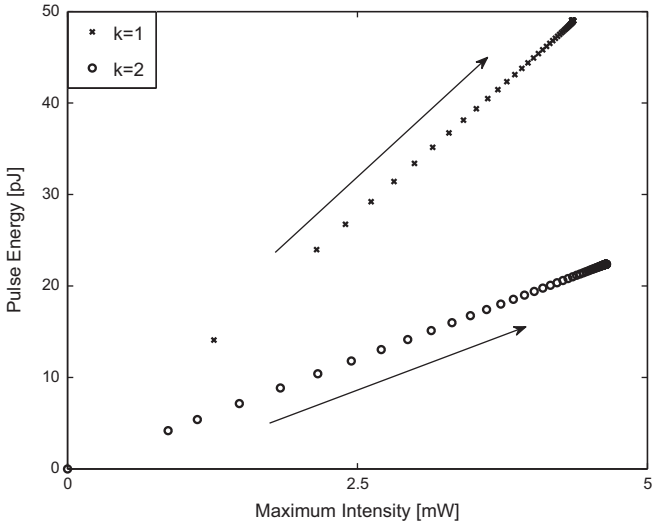

Fig. 5. Simulation of the pulse energy observed at the output of our model, as a function of the peak intensity and the length ratio.

have a central wavelength $\lambda_{FBG}=1553.55$ nm, a spectral bandwidth $\Delta\lambda_{3\ dB}=0.2$ nm and a reflectivity of 93%.

The temporal distribution of the output pulses from the fiber laser was obtained by employing a 50 GHz LeCroy WaveExpert 100 H sampling oscilloscope with a 10 GHz optical module, while spectral characteristics of all light sources were obtained by using the previously mentioned optical spectrum analyzer.

In order to obtain a stable and short pulse outputs with different repetition rates, we employed several values of L_A with $L_M=1.976$ m. Under the condition expressed in Eq. (1), a stable mode-locking regime is obtained, where the output frequency or round-trip frequency can be several times larger than the frequency corresponding to the active cavity ($f_{main}=52$ MHz). Fig. 6 shows typical pulse trains obtained when the auxiliary cavity length L_A was set to: (a) 1.976 m, (b) 0.988 m, (c) 0.659 m and (d) 0.494 m ($k=1$, 2, 3 and 4, respectively). The corresponding repetition rates were 52 MHz, 104 MHz, 156 MHz and 208 MHz, and the measured pulse widths for each case were about $T_{k=1}=3.5$ ns, $T_{k=2}=2.3$ ns, $T_{k=3}=1.6$ ns and $T_{k=4}=1.3$ ns. From these experimental results, it was observed that as L_A decreases (while maintaining fixed the main cavity length), the width of the output pulses also decreases and the pulse train frequency increases. As was analyzed in [25], for integer values of k, the repetition rate of the laser output can be calculated as $f_{laser}=kf_{main}$. In the cases where the system is not correctly adjusted (mismatch of lengths), for values of k different to an integer or rational, the observed output has a high frequency component modulated by the fundamental frequency defined by the length of the main cavity.

To complete the characterization of the APM fiber laser presented in this work, Fig. 7 shows the output power obtained for different values of the pump power. In this case, the auxiliary cavity length was $L_A=0.395$ m, that corresponds to $k=5$, so the laser was operating at 260 MHz. As it can be seen, a pulsed emission is obtained once the laser threshold is reached (approximately 10 mW). From there, it was observed a stable output of increasing amplitude and pulses with constant frequency and the same width (of about 1.2 ns), added to a small CW background. It is important to note that a very stable pulse train was obtained over a wide range of pumping powers.

Under a similar scheme, we have built another fiber laser with the same FBGs but with the main cavity length selected to be twice the length of the original one (i.e. $2L_M=3.952$ m). This was done by adding a piece of erbium doped fiber. The main frequency of this laser was $f_{main}=26$ MHz, and the output frequencies obtained by varying the auxiliary cavity length were $f_{laser}=26\times 10^6 k$ [Hz] (k as an integer number), i.e. 26 MHz, 52 MHz, 78 MHz,

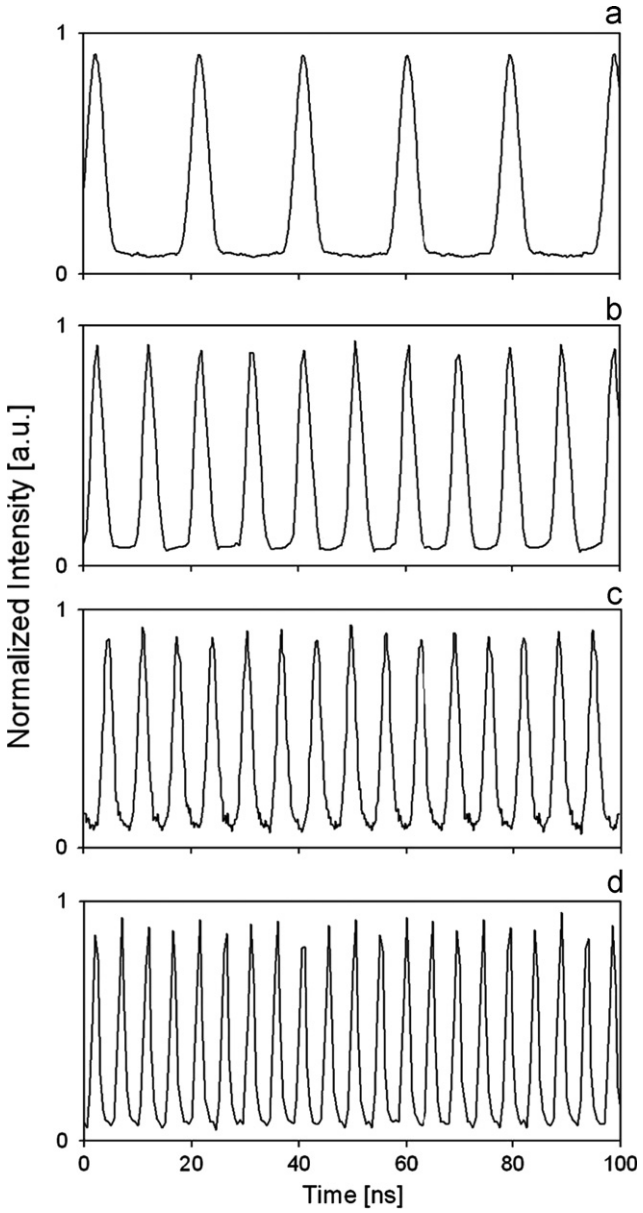

Fig. 6. Constant amplitude pulsed laser emission obtained for different values of L_A. (a) 1.976 m, (b) 0.988 m, (c) 0.659 m and (d) 0.494 m.

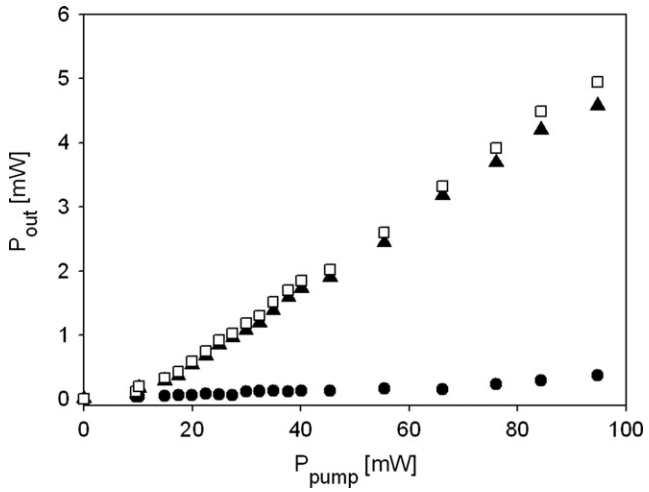

Fig. 7. Power evolution of the APM fiber laser as a function of the pump power. • is the CW component, ▲ pulsed component and □ laser output (CW+ pulsed).

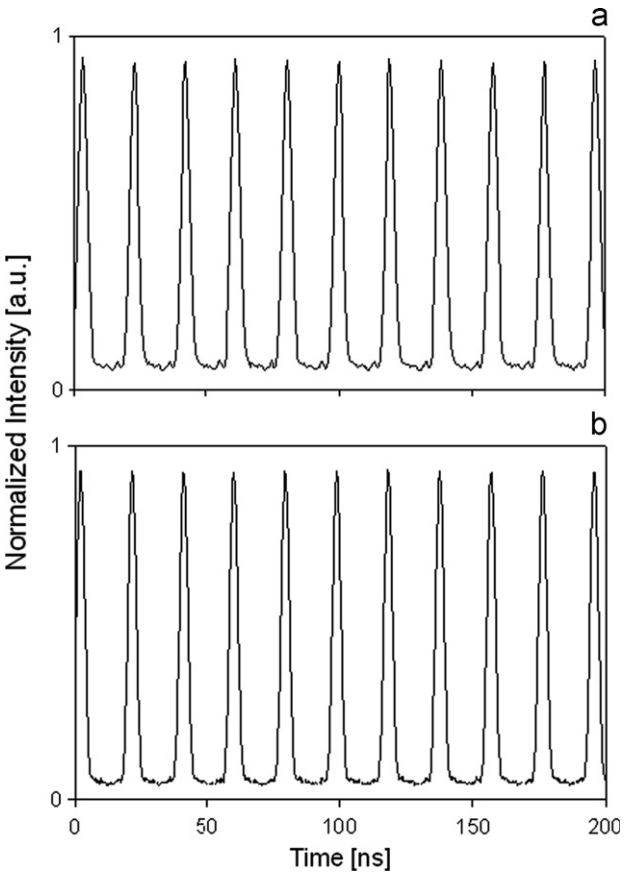

Fig. 8. Fiber laser emission pulsed at 52 MHz and obtained for: (a) $L_M = 5.928$ m, $L_A = 1.976$ m ($k = 3$); (b) $L_M = 3.952$ m, $L_A = 1.976$ m ($k = 2$).

104 MHz, 130 MHz, etc. In the same way, we have constructed a third APM fiber laser with an active cavity three times larger than the original one ($3L_M = 5.928$ m), whose main frequency was $f_{main} = 17.33$ MHz, and the output was pulsed at 17.33 MHz, 34.66 MHz, 52 MHz, 69.33 MHz, for $k = 1$, 2, 3 and 4, respectively, when the pigtail length was changed. As it can be seen, there are some output frequencies that are common with that of the original laser. For example, when L_A was set to 1.976 m, we obtained pulsed outputs of 52 MHz and 3.5 ns for all lasers, obviously for different values of k in each case. This results are plotted in Fig. 8, which shows that the width of the output pulses depends on the value of L_A, which in turn must satisfy the relation of Eq. (1).

In Fig. 9 we show the relationship between the pulse width and the repetition frequency of the laser output. The dashed line indicates a power regression of the experimental values which it is defined by $T_{pulse} = 1337 \times 10^{-3} f^{-0,7226} + 1045 \times 10^{-10}$ for the reflectivity values employed (around 93%), where T_{pulse} is the pulse width and f is the frequency. It should be noted that this plot includes experimental results obtained from other lasers made with active cavities lengths twice and three times grater than the original one (i.e. $2L_M = 3.952$ m and $3L_M = 5.928$ m). The pulse widths obtained for all lasers developed, showed the same behavior and can therefore be included in the same trace in Fig. 9. Considering these experimental results it could be inferred that the change in the temporal pulse width observed in [25] is related to the change of the FBG (reflectivity values and spectral positions). This point is to be investigated in a future work. In all the cases when the pigtail reflection is quenched (i.e. gel matching or

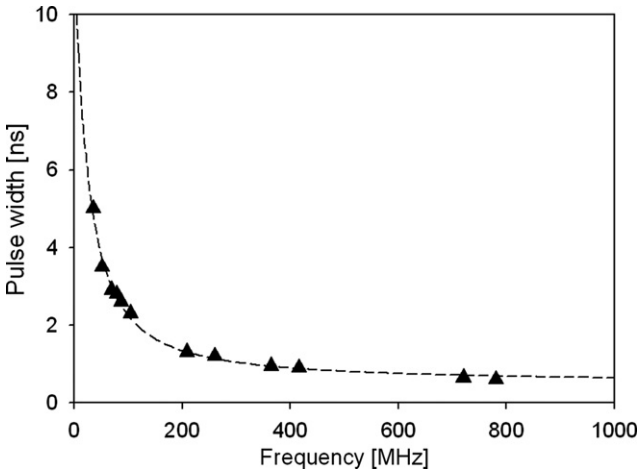

Fig. 9. Experimental output pulse widths as a function of the repetition frequency.

micro-curving of fiber), laser oscillation from the main cavity is observed at the corresponding fundamental frequency but with larger temporal pulse width values respect to the coupled cavities.

5. Discussion

To make a comparison between simulated and experimental results, we can observe the corresponding pulse widths in Figs. 4 and 6, respectively. Numerical results showed a very good correspondence with the experimental ones. The maximum error deviation between them was about 10%.

In order to analyze the influence of linear and non-linear processes, the main cavity length was first changed to $2L_M$ and then to $3L_M$. For both lasers we employed the appropriate auxiliary cavity length to obtain the same output frequencies, and they showed similar behaviors. Numerical results are plotted in Fig. 10(a,b) for laser outputs pulsed at 52 MHz. These results can be compared with the experimental ones showed in Fig. 8. The differences between the values obtained for the pulse widths were in the order of 1%. The absolute error in the measurements of the pulse widths observed in Figs. 6, 9 and 8 was less than 50 ps, while the simulation errors for most cases were not larger than this bound. As can be observed, no significant changes in the pulse width for laser outputs of the same frequency were obtained. In this case, we assume that, due to the pulse width values involved, the dispersion of the fibers plays a secondary role. On the other hand, the spectral broadening (related to the Kerr effect) obtained from the application of the model, could not be experimentally measured due to the limit imposed by the optical spectrum analyzer, whose spectral resolution is approximately 20 pm.

Fig. 11 shows the laser conversion efficiency η derived from Fig. 9 and that can be compared with the results obtained from the simulation, which are approximated by $\eta = 1.421 \times 10^{-6} f^{0.4677} + 4.352 \times 10^{-3}$. A comparison was made between this approximation and a power regression of the experimental results, and we found a small difference of about 3% between both slopes.

6. Conclusions

The proposed numerical model, based on SSM and TMM, allows to calculate a stable solution for the APM fiber laser here

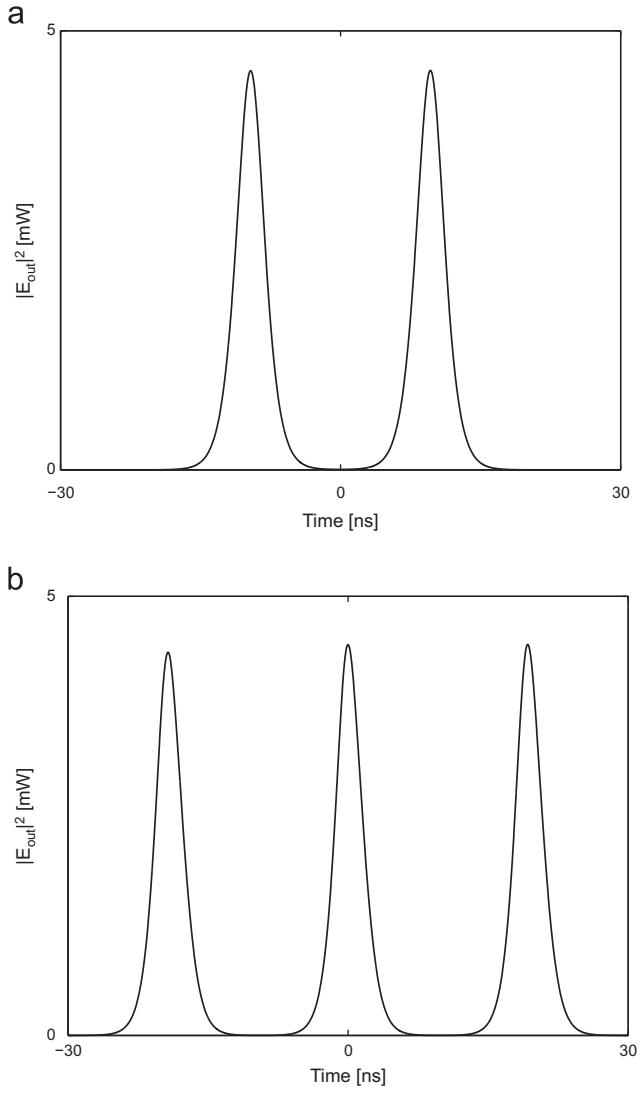

Fig. 10. Simulated fiber laser emission pulsed at 52 MHz. (a) $2L_M$ and $k=2$ (pulse width 3.46 ns) and (b) $3L_M$ and $k=3$ (pulse width 3.48 ns).

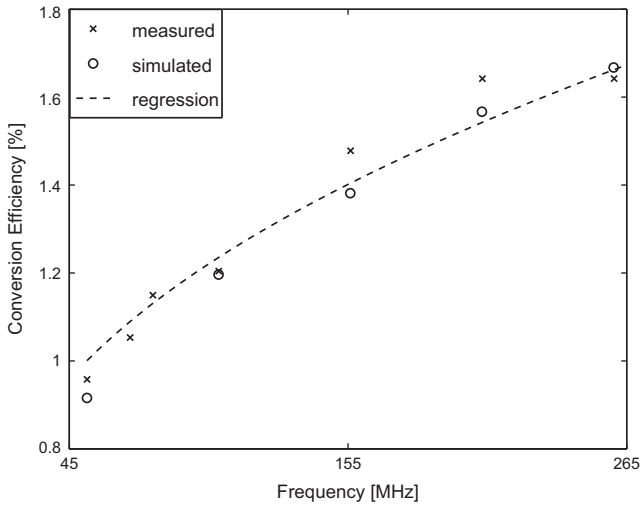

Fig. 11. Laser conversion efficiency as a function of the frequency, for the analyzed cases.

studied. The advantages of these methods applied in our model are great flexibility and easy implementation of the algorithms for the different cases that can be analyzed. The presented model supports the full profiles of the FBGs, reduces the computational cost and allows to obtain accurate results.

The shape of the output pulses mainly depends on both, the matching condition for the cavities lengths and the particular values chosen for the parameters, specially of the FBGs selected. Besides, it was found that the coupling effect in APM becomes more noticeable when the reflectivity value $|\rho_3|^2 \gg 0.04$, where a strong feedback is produced. However, a lower feedback is able to warrant a certain stability in the system. This is very important for many applications mainly related with communications and metrology. Our model also supports a stable solution for $|\rho_3|^2 = 0$, which corresponds to the case where the auxiliary cavity is decoupled from the main cavity. This behavior was discussed in Section 4.

Experimental results showed that the temporal width is univocally related to the pulse repetition frequency. The general effects of the dispersion are not strong because the fiber lengths are small (a few meters), and the temporal widths are in the range of nanoseconds. Moreover, the intensity of these pulses, even within the active cavity with moderate pump powers (of about 100 mW) are enough to warrant the presence of the Kerr effect in the system.

Regarding the potential of the proposed model, in particular based on the SSM with variable step, we expect some improvements in the modeling of APM laser systems including complex processes as the FWM and XPM. Moreover, the harmonic generation could be analyzed for no-integer relationships between the cavities lengths as that observed in [25], or in APM ultra-short pulses modeling.

Acknowledgments

This work was funded by Consejo Nacional de Investigaciones Científicas y Tecnológicas CONICET (PIP 112-200801-01769); Facultad de Ingeniería, Universidad Nacional de La Plata UNLP (Proy. 11/I169) and Comisión de Investigaciones Científicas de la Provincia de Buenos Aires CIC (Resolución no. 2410/12). E. Paulucci is a doctoral student in UNLP and has a fellowship of CONICET.

References

[1] Jiang M, Ahn K, Cao X, Dasika P, Liang Y, Islam M, et al. Synchronization of passively mode-locked erbium-doped fiber lasers and its application to optical communication networks. Journal of Lightwave Technology 1997;15:2020–8.
[2] Yoshida E, Shimizu N, Nakazawa M. A 40-GHz 0.9-ps regeneratively mode-locked fiber laser with a tuning range of 1530–1560 nm. IEEE Photonics Technology Letters 1999;11(12):1587–9.
[3] Je Y, Cundiff S. Femtosecond optical frequency comb: principle, operation and applications. Boston: Springer, Springer Science Business Media, Inc., 2005.
[4] Ablowitz M, Horikis T, Nixon S. Soliton strings and interactions in mode-locked lasers. Optics Communications 2009;282:4127–35.
[5] Laporta P, Longhi S, Marchesi M, Taccheo S, Svelto O. 2.5 GHz and 5 GHz harmonic mode-locking of a diode-pumped bulk erbium-ytterbium glass laser at 1.5 microns. Photonics Technology Letters 1995;7:155–7.
[6] Huang D, Lin G, Yang C. Fiber bragg based self matched additive pulse mode locked fiber lasers. Quantum Electronics 1999;35:138–46.
[7] Nielsen C, Andersen T, Keiding S. Stability analysis of an all fiber coupled cavity fabry perot additive pulse mode locked laser. Journal of Quantum Electronics 2005;41:198–204.
[8] Nishizawa N, Takahashi K. Time-domain near-infrared spectroscopy using a wavelength-tunable narrow-linewidth source by spectral compression of ultrashort soliton pulses. Optics Letters 2011;36(19):3780–2.
[9] Nicholson J, Yablon A, Yan M, Wisk P, Fleming J, Monberg E, et al. CLEO/QELS 2008 conference on the impact of nonlinearity during femtosecond pulse compression in fibers on continuum coherence. In: Lasers and electro-optics, 2008 and 2008 conference on quantum electronics and laser science; 2008. p. 1–2 .
[10] Inoue T, Tobioka H, Igarashi K, Namiki S. Optical pulse compression based on stationary rescaled pulse propagation in a comblike profiled fiber. Journal of Lightwave Technology 2006;24(7):2510–22.
[11] Williams J, Sugden K, Zhang L, Bennion I, Doran N. In-fiber grating systems for pulse compression and complete dispersion compensation. In: IEE Colloquium on optical fibre gratings and their applications; 1995. p. 9/1–9/6.
[12] Hideur A, Chartier T, Brunel M, Salhi M, Ozkul C, Sanchez F. Mode-lock, q-switch and cw operation of an yb-doped double-clad ber ring laser. Optics Communications 2001;198:141–6.
[13] Engelbrecht M, Haxsen F, Ruehl A, Wandt D, Kracht D. 320-fs thulium-doped fiber-ring-laser with a pulse energy of 3.5-nj. In: Conference on lasers and electro-optics/quantum electronics and laser science conference and photonic applications systems technologies, OSA; 2008. p. CFD4.
[14] Nakazawa M, Yoshida E. A 40-GHz 850-fs regeneratively fm mode-locked polarization-maintaining erbium fiber ring laser. IEEE Photonics Technology Letters 2000;12(12):1613–5.
[15] Haus H, Fujimoto J, Ippen E. Structures for additive pulse mode locking. Optic Communications 1991;8:2068–76.
[16] Haus H. Mode locking of lasers. Selected Topics in Quantum Electronics 2000;6:1173–85.
[17] Matsko AB, Savchenkov AA, Maleki L. Normal group-velocity dispersion kerr frequency comb. Optics Letters 2012;37(1):43–5.
[18] Han Y-G, Tran TVA, Lee SB. Wavelength-spacing tunable multiwavelength erbium-doped fiber laser based on four-wave mixing of dispersion-shifted fiber. Optics Letters 2006;31(6):697–9.
[19] Schröder J, Coen S, Vanholsbeeck F, Sylvestre T. Passively mode-locked raman fiber laser with 100 GHz repetition rate. Optics Letters 2006;31(23):3489–91.
[20] Agrawal G. Nonlinear fiber optics. San Diego, California: Academic Press; 1995.
[21] Farnum ED, Butson L, Kutz JN. Theory and simulation of dual-frequency mode-locked lasers. Journal of the Optical Society of America B 2006;23:257–64.
[22] Geisler T, Shore K, Soerensen M, Christiansen P, Mark J. Nonlinear fiber external cavity mode locking of erbium doped fiber lasers. Journal of the Optical Society of America B 1993;10:1166–74.
[23] Kashyap R. Fiber bragg gratings. New York: Academic Press; 1999.
[24] Saleh BEA, Teich MC. Fundamentals of photonics. New York, NY: John Wiley & Sons; 2007.
[25] Russo N, Duchowicz R. High frequency pulse trains from a self-starting additive pulse mode-locked all-fiber laser. Optics Communications 2010;283:113–7.
[26] Sinkin OV, Holzlöhner R, Zweck J, Menyuk CR. Optimization of the split-step fourier method in modeling optical-fiber communications systems. Journal of Lightwave Technology 2003;21(1):61.
[27] Desurvire E. Erbium-doped fiber amplifiers. New York, NY: John Wiley & Sons; 1994.
[28] Martinez OE, Fork RL, Gordon JP. Theory of passively mode-locked lasers for the case of a nonlinear complex-propagation coefficient. Journal of the Optical Society of America B 1984;2:753–60.
[29] Martinez OE, Fork RL, Gordon JP. Theory of passively mode-locked lasers including self-phase modulation and group-velocity dispersion. Optics Letters 1984;9:156–8.
[30] Ziemer R, Tranter W. Principles of communications. New York, NY: John Wiley & Sons, 2008.
[31] Paulucci E, Russo N, Sicre E, Duchowicz R. Theory and simulation of a two coupled-cavities fiber laser. In: 22nd congress of the international commission for optics: light for the development of the world, 2011.